Building-Block-Flow Model for Large-Eddy Simulation: Application to the NASA CRM-HL

A. Lozano-Durán*, G. Arranz† and Y. Ling‡
Department of Aeronautics and Astronautics, Massachusetts Institute of Technology, Cambridge, MA, 02139

We perform wall-modeled large-eddy simulation (WMLES) of the NASA Common Research Model High-Lift (CRM-HL) using the Building-block Flow Model (BFM) [1]. BFM is a unified subgrid-scale (SGS) and wall model for WMLES that devises the flow as a collection of building blocks. The model is rooted in the assumption that simple canonical flows contain the essential physics to provide accurate predictions in more complex scenarios [2]. BFM is implemented via artificial neural networks (ANNs) and accounts for a limited set of laminar flows, wall-attached turbulence, adverse pressure gradient effects, and separation. The model uses a Bayesian classifier, which identifies the contribution of each building block in the flow, and an ANN-based predictor, which estimates the eddy viscosity based on the building-block units. The training data are directly obtained from WMLES with an exact SGS/wall model for the mean quantities to guarantee consistency with the numerical discretization and gridding strategy. Here, we validate the BFM in the NASA CRM-HL with an emphasis on grid resolutions that are affordable to attain fast turnaround times in the design cycle. We show that BFM offers improved and/or more consistent results in the prediction of the lift, drag, and pitching moment coefficients compared to conventional WMLES approaches, especially at high angles of attack. Future versions of the BFM will incorporate additional building-block flows to enhance the predictive capabilities of the model.

I. Nomenclature

a_∞	=	free-stream sound speed
C_L	=	lift coefficient
C_D	=	drag coefficient
C_M	=	pitching moment coefficient
$\mathrm{d}P/\mathrm{d}x$	=	mean streamwise pressure gradient
h	=	half-height of the channel
I_i	=	i-th invariant of the gradient velocity tensor
M	=	U_∞/a_∞ Mach number
L_x, L_y, L_z	=	streamwise, wall-normal, and spanwise size of the channel
p	=	pressure
Re	=	Reynolds number
$\bar{\mathbf{R}}$	=	rate-of-rotation tensor
$\bar{\mathbf{S}}$	=	rate-of-strain tensor
U_∞	=	free-stream streamwise velocity
$u_\parallel$	=	magnitude of the velocity parallel to the wall
u_t	=	top wall velocity for turbulent Poiseuille-Couette flows
x	=	streamwise coordinate
y	=	vertical coordinate
z	=	spanwise coordinate
Δ	=	characteristic grid resolution
ν	=	kinematic viscosity
ν_t	=	eddy viscosity

*Draper Assistant Professor, Department of Aeronautics and Astronautics, adrianld@mit.edu, and AIAA Senior Member.
†Postdoctoral Associate, Department of Aeronautics and Astronautics, garranz@mit.edu, and AIAA Member.
‡Graduate Student, Department of Aeronautics and Astronautics, lingyn@mit.edu, and AIAA Student Member.

ρ	=	fluid density
τ_w	=	shear stress at the wall
PC	=	Poiseuille-Couette
EQWM	=	Equilibrium wall model
DSM	=	Dynamic Smagorinsky model
LES	=	Large-Eddy simulation
RANS	=	Reynolds-averaged Navier-Stokes
SGS	=	Subgrid-scale
WMLES	=	Wall-modeled Large-Eddy simulation

II. Introduction

Computational Fluid Dynamics (CFD) stands as an essential tool for the design and optimization of aero/hydro-vehicles relevant to the industry. However, CFD of realistic vehicles poses a unique challenge due to the ubiquity of complex flow physics. Among the most pressing challenges, we can cite turbulent flows in the presence of adverse pressure-gradient effects, flow separation, shockwaves, laminar-to-turbulent transition, and strong mean unsteadiness, to name a few [3, 4]. While there are CFD models that are accurate in predicting one or two particular scenarios, no model is capable of performing accurately across all the flow phenomena described above [5, 6]. The limitations above raise the following question: how to devise a unified CFD closure model capable of accounting for a rich collection of flow physics?

In the present work, we address this challenge by using the Building-block Flow Model (BFM) for large-eddy simulation (LES) [7]. BFM is a unified SGS and wall model for LES that devises the flow as a collection of building blocks. The core assumption of the model is that simple canonical flows contain the essential physics to provide accurate predictions in more complex flows [1, 2]. It is also envisaged to provide accurate results with coarse resolutions which are affordable for industrial applications.

The BFM is developed with the framework of wall-modeled LES (WMLES), which has recently gained momentum as a tool for aerospace applications [8]. Goc et al. [9] have shown that WMLES is approaching the accuracy and computational efficiency demanded by the aerospace industry. While state-of-the-art WMLES performs satisfactorily in turbulent boundary layers with sufficient grid resolution, its performance deteriorates in the presence of less than 20 grid points per boundary layer thickness. Unfortunately, the latter grid resolution is typical for external aerodynamics applications [6, 10]. The results from the 4th High Lift Prediction Workshop [5] have also evidenced the deficiencies of state-of-the-art WMLES in the context of aircraft aerodynamics, e.g., error cancellation, non-monotonic grid convergence/independence, and lack of clear best practices, to name a few. Even meshes with more than 350 million control volumes, which are too costly for routine industrial design cycle, are unable to accurately predict the wind tunnel measurements. The goal of the BFM is to improve the accuracy and computational efficiency of WMLES across multiple flow regimes.

The BFM is implemented using artificial neural networks (ANNs) within the supervised learning paradigm, which has been extensively explored for modeling in recent years. For example, SGS models have been trained using data from filtered direct numerical simulation (DNS) [11, 12]. Examples of supervised learning for wall modeling include Yang et al. [13], Zhou et al. [14], Zangeneh [15] and Huang et al. [16], to name a few. Interestingly, most studies to date have trained the model with data from higher-fidelity simulations, such as DNS or wall-resolved LES. As a consequence, previous models ignored the nonnegligible errors arising from the numerical discretization in actual WMLES. An exception is the work by Bae and Koumoutsakos [17] using reinforcement learning. Here, we take advantage of a novel data preparation process to ensure numerical consistency between the training data and the model deployed in the flow solver. Additionally, most of the models cited above are limited to simple flow configurations and rely on information about the flow that is typically inaccessible in real-world applications, such as the boundary-layer thickness. One exception is the ML wall model introduced by Lozano-Durán and Bae [2], which is directly applicable to arbitrary complex geometries and provides the foundations for the BFM.

This paper is organized as follows. Section III details model formulation, training procedure, and simulation setup. Results for the CRM-HL are presented in Section IV. Finally, concluding remarks are offered in Section V.

III. Methodology

A. Model overview

The main modeling hypothesis of the BFM is that the SGS physics of complex flows can be locally mapped into the small scales of simpler canonical flows [7]. Therefore, the BFM is capable of accurately predicting the statistical properties of complex flows as long as the canonical flows used for training the model are representative of the (missing) SGS flow physics. A detailed discussion about the modeling assumptions of the BFM can be found in Lozano-Durán and Bae [2]. Here, we test the ability of a limited collection of simple canonical flows to model the flow over the CRM-HL. The model architecture is summarized in Fig. 1.

In the version of the model considered here*, the classifier categorizes the flow into different types of canonical flows, and the predictor provides the wall shear stress and eddy viscosity based on the likelihood of each category. Four types of building-block flows are considered: laminar channel flow, fully developed turbulent channel flow, turbulent Poiseuille-Couette flow with adverse pressure gradient, and turbulent Poiseuille-Couette flow with "separation".

The anisotropic component of the SGS stress tensor is given by the eddy-viscosity model

$$\bar{\tau} = -2\nu_t \bar{\mathbf{S}}, \tag{1}$$

where $\bar{\mathbf{S}}$ is the rate-of-strain tensor. The eddy viscosity is assumed to be a function of the invariants of the velocity gradient tensor [18]

$$\nu_t = f(I_1, I_2, I_3, I_4, I_5, I_6, \theta), \tag{2}$$

where f represents an ANN, and θ denotes additional input variables, namely, ν, Δ and $u_\parallel$, where ν is the kinematic viscosity, Δ is the characteristic grid size and $u_\parallel$ is the magnitude of the wall-parallel velocity measured with respect to the wall. The invariants of rate-of-strain and rate-of-rotation tensors ($\bar{\mathbf{R}}$) are defined as

$$\begin{aligned} I_1 &= \mathrm{tr}\left(\bar{\mathbf{S}}^2\right), & I_2 &= \mathrm{tr}\left(\bar{\mathbf{R}}^2\right), \\ I_3 &= \mathrm{tr}\left(\bar{\mathbf{S}}^3\right), & I_4 &= \mathrm{tr}\left(\bar{\mathbf{S}}\bar{\mathbf{R}}^2\right), \\ I_5 &= \mathrm{tr}\left(\bar{\mathbf{S}}^2\bar{\mathbf{R}}^2\right), & I_6 &= \mathrm{tr}\left(\bar{\mathbf{S}}^2\bar{\mathbf{R}}^2\bar{\mathbf{S}}\bar{\mathbf{R}}\right). \end{aligned} \tag{3}$$

The predictor is divided into two types of ANNs as shown in Fig. 2: a near-wall ANN and an outer-region ANN. The near-wall ANN is responsible for the control volumes in contact with the wall and utilizes the wall-parallel velocity as input. The predictions for the control volumes away from the wall are performed by the outer-region ANN. The mapping between inputs and output is learned from data generated from controlled WMLES simulations, which are detailed in Section III.B.

The input and output variables of the ANN are given in non-dimensional form. The non-dimensionalization of the input and output features is attained by using parameters that are local in both time and space to guarantee the applicability of the model to complex geometries. Two cases are considered. For the near-wall predictor, the input and output quantities are non-dimensionalized using viscous scaling (ν and Δ). For the outer-region predictor, the input and output variables are non-dimensionalized using semi-viscous scaling [$(\sqrt{2\bar{\mathbf{S}}:\bar{\mathbf{S}}}\nu)^{1/2}$ and Δ]. The BFM is implemented in charLES, a finite-volume, compressible flow solver with Voronoi gridding capabilities. Readers are referred to [9] for more details about charLES.

B. Building-block flows and data preparation

Figure 1 illustrates the collection of building-block flows. The Poiseuille flow is used to generally represent laminar flows. The turbulent channel flow models the regime where turbulence is fully developed without significant mean-pressure gradient effects. In both cases, the bottom and top walls are static. In the turbulent Poiseuille-Couette flows, the top wall moves at a constant speed (u_t) in the streamwise direction, and an adverse pressure gradient is applied in the direction opposed to the top wall velocity. The adverse pressure gradient ranges from mild to strong, so that the flow "separates" (i.e., zero wall shear stress) on the bottom wall.

The training data is generated using WMLES with an exact-for-the-mean eddy-viscosity and wall model denoted by ESGS. This enables the model to account for the numerical errors of the flow solver. More details about ESGS can be found in Lozano-Durán and Bae [2]. The ESGS model is based on the anisotropic minimum-dissipation SGS model [19] combined with a controller that iteratively adjusts the eddy viscosity to match the DNS mean velocity

*BFM-v0.1.0

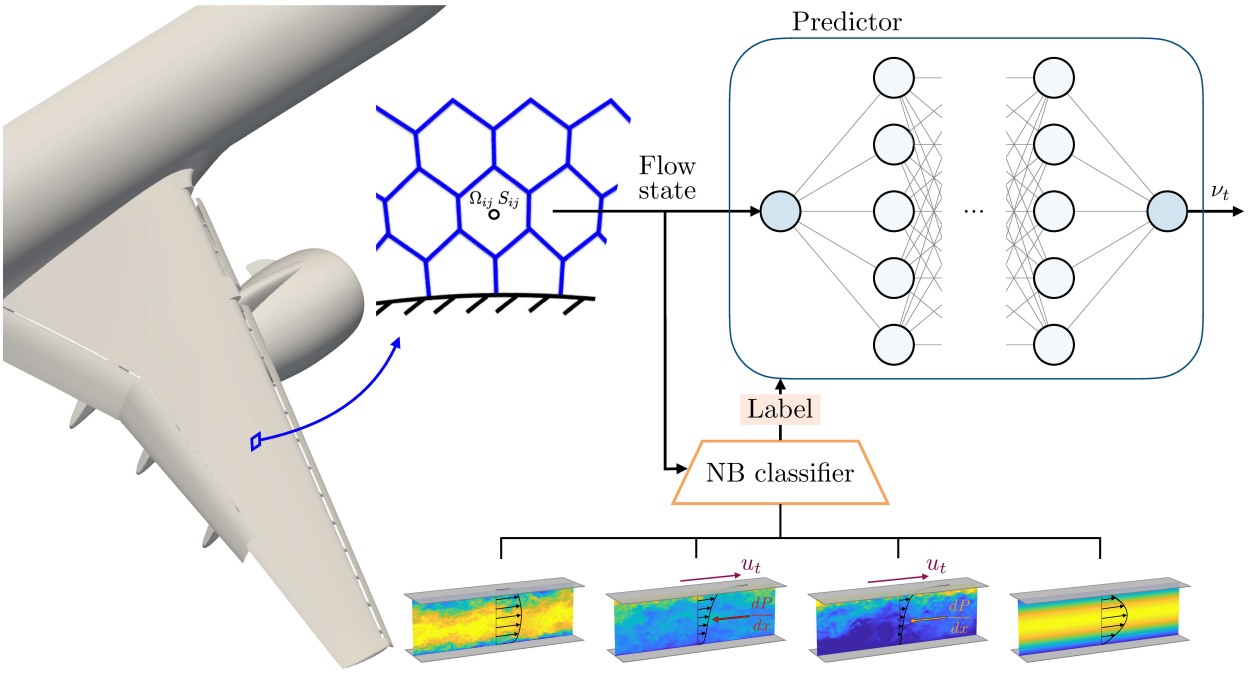

Fig. 1 Schematic of the building-block flow model (BFM). The panel shows the classifier-predictor structure and the ANN architecture. The flow state refers to $(I_1, ..., I_6, \nu, \Delta, u_{||})$ and different ANNs are used for the inner and outer layer. The bottom of the figure depicts the building-block flows considered (from left to right): turbulent channel flow, Poiseuille-Couette flow with mild adverse pressure gradient, Poiseuille-Couette flow with separation, and laminar Poiseuille flow.

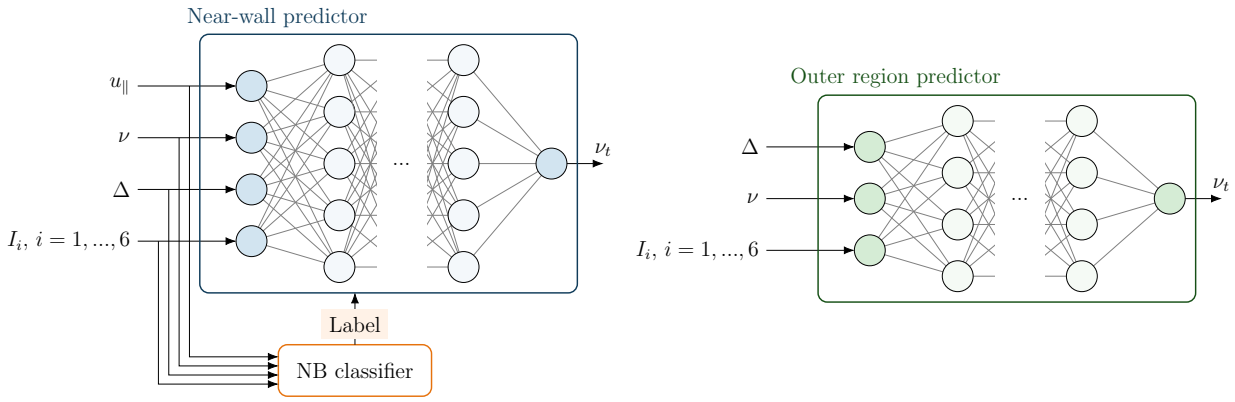

Fig. 2 Schematic of the two types of ANNs used by the building-block flow model.

Case	Re_τ	L_x/h	L_z/h	Re_p
C550	547	4π	2π	N/A
C950	943	4π	2π	N/A
C2000	2003	4π	2π	N/A
4200	4179	4π	2π	N/A
PC0	6	2π	π	680
PC100	120	2π	π	340

Table 1 Parameters of the controlled WMLES used for training the BFM. The cases are labeled as C[Re_τ] for turbulent channel flows and as PC[Re_τ] for turbulent Poiseuille-Couette flows. Re_τ is the friction Reynolds number. For turbulent PC flow, Re_τ is based on the shear stress of the bottom wall. L_x and L_z are streamwise and spanwise length of the channel, and h is the channel height. The grid size of WMLES is $N_x \times N_y \times N_z = 66 \times 12 \times 34$ for all cases. The laminar cases used for training are not included in the table.

profile. A Dirichlet non-slip boundary condition is applied at the walls and the correct wall shear stress is enforced by augmenting the eddy viscosity at the walls such that

$$\nu_t|_w = \left(\frac{\partial \bar{u}}{\partial y}\right)\Big|_w^{-1} \frac{\tau_w}{\rho} - \nu \tag{4}$$

following Bae and Lozano-Durán [20]. For turbulent channel flows, the mean DNS quantities are obtained from the database by Jimenéz and coworkers [21–23]. Four cases with friction Reynolds numbers 550, 950, 2000 and 4200 are used. For the turbulent Poiseuille-Couette flows, our in-house code is used to generate DNS data [24]. Two cases (labeled as PC0 and PC100) are considered, which correspond to separation and adverse pressure gradient, respectively. The Reynolds numbers based on the adverse pressure gradient are $Re_P = \sqrt{h^3 \mathrm{d}P/\mathrm{d}x}/\nu = 680$ and 340, and the Reynolds number based on the top wall velocity is $Re_U = u_t h/\nu = 22,360$. The computational domain is $L_x \times L_y \times L_z = 4\pi h \times 2h \times 2\pi h$ for channel flows and $L_x \times L_y \times L_z = 2\pi h \times 2h \times \pi h$ for PC-0 and PC-2, where h is the channel half-height. The grid size for the WMLES cases with ESGS is $\Delta \approx 0.2h$. The Table 1 provides a summary of the cases used for training.

C. Predictor and classifier

The ANN architecture for the predictors is a fully connected feedforward neural network with 6 hidden layers and 40 neurons per layer. The ANNs were trained using stochastic gradient descent by randomly dividing training data into two groups, the training set (80% of the data) and test set (20% of the data). For laminar flows, the eddy viscosity is set to zero.

The classification of the flow at a given point is done in two steps. First, the flow is classified as turbulent or laminar. If the flow is turbulent, it is further classified as zero-pressure-gradient wall turbulence (ZPG), adverse-pressure-gradient wall turbulence (APG), or separated turbulent flow. A Naive Bayes classifier is employed whose inputs are the non-dimensionalized invariants (together with $u_\parallel$ for the second classification). For the first classification, the invariants are normalized with ν and Δ, whereas for the second classification, $\sqrt{2\bar{\mathbf{S}} : \bar{\mathbf{S}}}$ is used. The output of the classifier is a label that is fed to the predictor, as shown in Fig. 1.

The classifier is trained with the same cases as the predictor in addition to synthetic data generated for laminar Poiseuille flow at $Re_\tau = [5 - 150]$. The classifier is applied to all grid points to discern between turbulent and laminar flow. The second classification is only applied to the points in contact with the wall. Fig. 3 shows the confusion matrix for the classifier. The classifier shows 100% accuracy in the first classification. The numbers in the cells indicate the

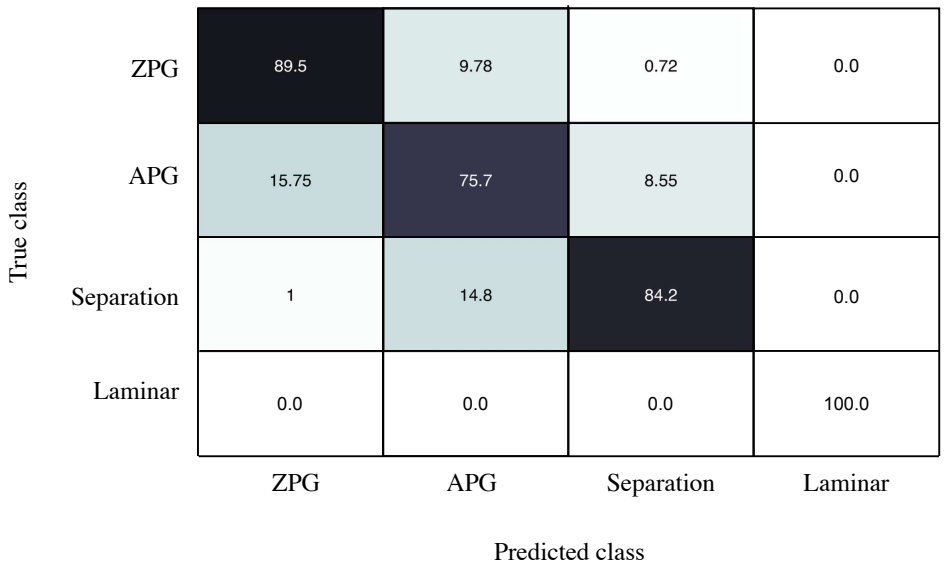

Fig. 3 Confusion matrix of the classifier for the first grid point off wall.

percentage of samples that are classified as a given class, showing that flows are predicted with > 75% accuracy. ZPG and separated flow are predicted with > 80% accuracy, whereas the classification of APG flow exhibits lower accuracy.

D. Case description and computational set-up

The NASA CRM-HL is a geometrically complex aircraft that includes the bracketry associated with deployed flaps and slats as well as a flow-through nacelle mounted on the underside of the wing. The simulations are performed in free air at the Reynolds number of 5.49 million based on the mean aerodynamic chord and freestream velocity. The freestream Mach number is 0.20. The results are compared with wind tunnel experimental data from Evans et al. [25] corrected for free air conditions. Further details of the experimental set-up can be found in Lacy and Sclafani [26].

We follow the computational setup from Goc et al. [27]. A semi-span aircraft geometry is simulated and the symmetry plane is treated with free-slip and no penetration boundary conditions. A uniform plug flow is used as the inlet. A non-reflecting boundary condition with specified freestream pressure is imposed at the outlet [28]. The total number of grid points is 40 million and the number of grid points per boundary layer thickness ranges from zero to twenty. The reader is referred to Goc et al. [27] for more details about the gridding strategy.

We perform simulations of the CRM-HL using BFM at two angles of attack, $\alpha = 7.05^\circ$ and 19.57°, and compare the lift, drag and pitching moment coefficients with experimental data and simulations from Goc et al. [27] using Dynamic Smagorinsky model with the equilibrium wall model, labeled as DSM-EQWM. A slice of the grid is depicted in Fig. 4.

IV. Results

Figure 5 displays the lift (C_L), drag (C_D), and pitching moment (C_M) coefficients for BFM and DSM-EQWM compared to experimental results. For $\alpha = 7.05^\circ$, DSM-EQWM correctly predicts C_L and C_D. However, further analysis has shown that this accurate prediction is coincidental and due to error cancellation when integrating the total forces [27]. This is corroborated by the poor predictions of pitching moment by DSM-EQWM. The case of $\alpha = 19.57^\circ$ corresponds to the angle of attack of maximum lift coefficient. DSM-EQWM underpredicts the C_L, whereas the BFM accurately predicts C_L. The drag coefficient is overpredicted by both models, but the pitching moment computed using the BFM is closer to the experimental values, suggesting that the BFM provides a more accurate distribution of the forces over the wing. Inspection of the sectional pressure coefficient, shown in Fig. 6, indicates that the BFM maintains the flow attached over a longer section of the wing compared to DSM-EQWM, which explains the enhanced performance

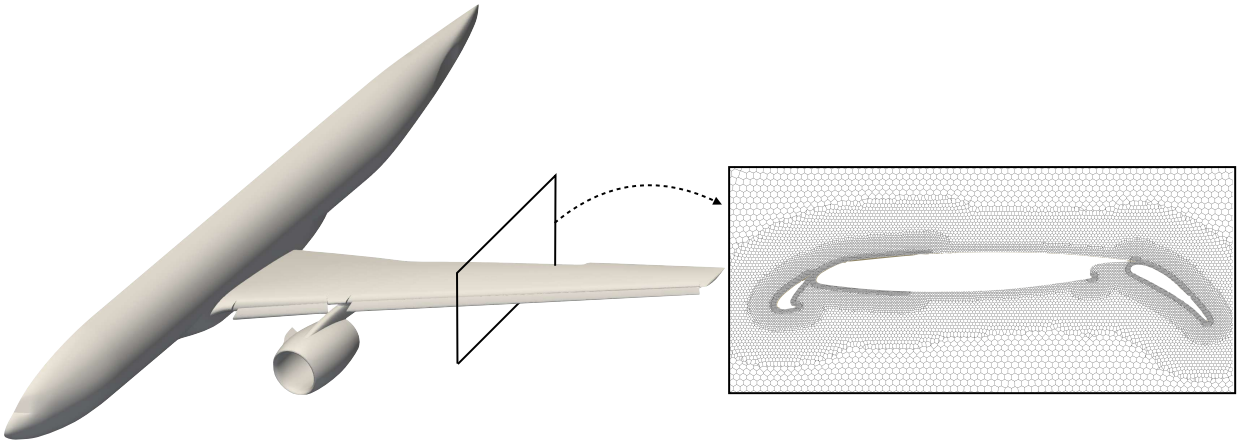

Fig. 4 Geometry of the CRM-HL model and a cross-sectional view of the grid over the wing surface.

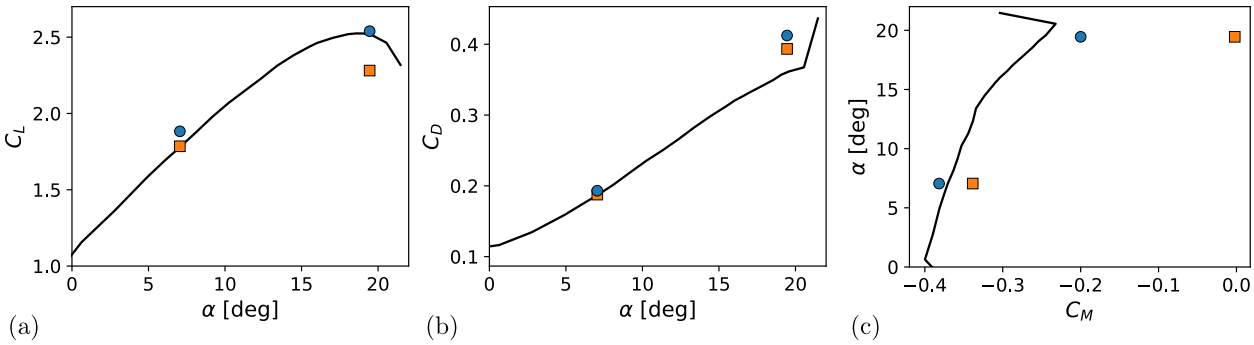

Fig. 5 (a) Lift, (b) drag and (c) pitching moment coefficients for CRM-HL. The black lines denote experimental results, squares are for DSM-EQWM and circles are for the BFM.

of the BFM. Overall, the BFM offers improved and/or more consistent results than DSM-EQWM, especially close to the stall. It is worth remarking that BFM has never 'seen' an aircraft-like flow or been trained in a case that resembles an airfoil or a wing.

V. Conclusions

We have examined the performance of the building-block flow model (BFM)[†] [1] for large-eddy simulation in the NASA Common Research Model. The model is devised to address the challenges faced by CFD in the industry, i.e., the need for accurate and robust solutions at an affordable computational cost. The core assumption of the BFM is that the subgrid-scale physics of complex flows can be mapped into the physics of simpler canonical flows [2, 7].

The BFM comprises two components: one classifier and one predictor. The classifier is trained to place the flow into separate categories, while the predictor outputs the modeled SGS/wall stress based on the likelihood of each category. Unlike previous models, the training data are directly obtained from controlled WMLES with an 'exact' model for the mean quantities of interest to guarantee consistency with the numerical discretization and grid structure of the solver. The model is applicable to complex geometries and is implemented using artificial neural networks. In the current version tested, the model has been trained using a limited set of data from turbulent channel flows at different Re_τ and turbulent Poiseuille-Couette flows with varying adverse pressure gradient and laminar flow.

The performance of the BFM in complex scenarios was evaluated in the NASA Common Research Model High-

[†]BFM-v0.1.0

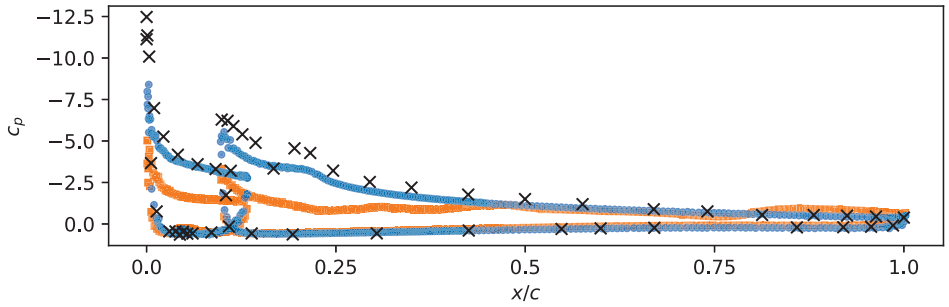

Fig. 6 Pressure coefficient at the 82% spanwise section of the wing for $\alpha = 19.57°$. Black $\times$ represents experimental results, orange squares are for DSM-EQWM and blue circles are for the BFM.

Lift (CRM-HL). We have shown that, for the coarse resolution considered here, the BFM offers improvements in the prediction of lift, drag, and pitching momentum coefficients compared to conventional SGS/wall models, especially at high angle of attack. The main exceptions are the coincidentally accurate predictions of the lift coefficient by conventional SGS/wall models due to error cancellation. To improve model performance, we will continue the training of future versions of the BFM with additional cases to account for a richer collection of flow physics.

Acknowledgments

The authors acknowledge the support of the CTR Summer Program 2022 at Stanford University. The authors also acknowledge the Massachusetts Institute of Technology, SuperCloud, and Lincoln Laboratory Supercomputing Center for providing HPC resources that have contributed to the research results reported here. G. A. was partially supported by STTR grant no. N68335-21-C-0270 NAVAIR - Cascade Technologies.

References

[1] Ling, Y., Arranz., G., Williams., E., Goc, K., Griffin, K., and Lozano-Durán, A., "WMLES based on building block flows," *Proceedings of the Summer Program, Center for Turbulence Research , Stanford University*, 2022.

[2] Lozano-Durán, A., and Bae, H. J., "Machine-learning building-block-flow wall model for large-eddy simulation," , 2023.

[3] Casey, M., Wintergerste, T., European Research Community on Flow, T., and Combustion., *ERCOFTAC best practice guidelines: ERCOFTAC special interest group on "quality and trust in industrial CFD"*, ERCOFTAC, 2000.

[4] Slotnick, J., Khodadoust, A., Alonso, J., Darmofal, D., Gropp, W., Lurie, E., and Mavriplis, D., "CFD Vision 2030 Study: A Path to Revolutionary Computational Aerosciences," *Technical Report, NASA/CR-2014-218178, NF1676L-18332*, 2014.

[5] GMGW-HLPW, "4th CFD High Lift Prediction Workshop," , 2022. URL `https://hiliftpw.larc.nasa.gov/Workshop4/WorkshopPresentations/08-09_GMGW3_HLPW4_Summary.pdf`.

[6] Lozano-Durán, A., Bose, S. T., and Moin, P., "Performance of Wall-Modeled LES with Boundary-Layer-Conforming Grids for External Aerodynamics," *AIAA J.*, Vol. 60, No. 2, 2022, pp. 747–766. https://doi.org/10.2514/1.J061041.

[7] Lozano-Durán, A., and Bae, H. J., "Self-critical machine-learning wall-modeled LES for external aerodynamics," *Center for Turbulence Research - Annual Research Briefs*, 2020, pp. 197–210.

[8] Bose, S. T., and Park, G. I., "Wall-Modeled LES for Complex Turbulent Flows," *Annu. Rev. Fluid Mech.*, Vol. 50, No. 1, 2018, pp. 535–561. https://doi.org/10.1146/annurev-fluid-122316-045241.

[9] Goc, K. A., Lehmkuhl, O., Park, G. I., Bose, S. T., and Moin, P., "Large eddy simulation of aircraft at affordable cost: a milestone in computational fluid dynamics," *Flow*, Vol. 1, 2021.

[10] Lozano-Durán, A., and Bae, H. J., "Error scaling of large-eddy simulation in the outer region of wall-bounded turbulence," *J. Comp. Phys.*, Vol. 392, 2019, pp. 532–555.

[11] Gamahara, M., and Hattori, Y., "Searching for turbulence models by artificial neural network," *Phys. Rev. Fluids*, Vol. 2, No. 5, 2017, p. 054604.

[12] Xie, C., Wang, J., Li, H., Wan, M., and Chen, S., "Artificial neural network mixed model for large eddy simulation of compressible isotropic turbulence," *Phys. Fluids*, Vol. 31, No. 8, 2019, p. 085112.

[13] Yang, X., Zafar, S., Wang, J.-X., and Xiao, H., "Predictive large-eddy-simulation wall modeling via physics-informed neural networks," *Phys. Rev. Fluids*, Vol. 4, No. 3, 2019, p. 034602.

[14] Zhou, Z., He, G., and Yang, X., "Wall model based on neural networks for LES of turbulent flows over periodic hills," *Phys. Rev. Fluids*, Vol. 6, No. 5, 2021, p. 054610.

[15] Zangeneh, R., "Data-driven model for improving wall-modeled large-eddy simulation of supersonic turbulent flows with separation," *Phys. Fluids*, Vol. 33, No. 12, 2021, p. 126103. https://doi.org/10.1063/5.0072550.

[16] Huang, X. L. D., Yang, X. I. A., and Kunz, R. F., "Wall-modeled large-eddy simulations of spanwise rotating turbulent channels–Comparing a physics-based approach and a data-based approach," *Phys. Fluids*, Vol. 31, No. 12, 2019, p. 125105. https://doi.org/10.1063/1.5129178.

[17] Bae, H. J., and Koumoutsakos, P., "Scientific multi-agent reinforcement learning for wall-models of turbulent flows," *Nature Comm.*, Vol. 13, No. 1, 2022, pp. 1–9.

[18] Lund, T. S., and Novikov, E. A., "Parameterization of subgrid-scale stress by the velocity gradient tensor," *Annual Research Briefs, 1992*, 1993.

[19] Rozema, W., Bae, H. J., Moin, P., and Verstappen, R., "Minimum-dissipation models for large-eddy simulation," *Phys. Fluids*, Vol. 27, No. 8, 2015, p. 085107.

[20] Bae, H. J., and Lozano-Durán, A., "Effect of wall boundary conditions on a wall-modeled large-eddy simulation in a finite-difference framework," *Fluids*, Vol. 6, No. 3, 2021, p. 112.

[21] Del Alamo, J. C., Jiménez, J., Zandonade, P., and Moser, R. D., "Scaling of the energy spectra of turbulent channels," *J. Fluid Mech.*, Vol. 500, 2004, pp. 135–144. https://doi.org/10.1017/S002211200300733X.

[22] Hoyas, S., and Jiménez, J., "Scaling of the velocity fluctuations in turbulent channels up to $Re_\tau = 2003$," *Phys. Fluids*, Vol. 18, No. 1, 2006, p. 011702. https://doi.org/10.1063/1.2162185.

[23] Lozano-Durán, A., and Jiménez, J., "Effect of the computational domain on direct simulations of turbulent channels up to $Re_\tau = 4200$," *Phys. Fluids*, Vol. 26, No. 1, 2014, p. 011702. https://doi.org/10.1063/1.4862918.

[24] Lozano-Durán, A., Giometto, M. G., Park, G. I., and Moin, P., "Non-equilibrium three-dimensional boundary layers at moderate Reynolds numbers," *J. Fluid Mech.*, Vol. 883, 2020, p. A20. https://doi.org/10.1017/jfm.2019.869.

[25] Evans, A. N., Lacy, D. S., Smith, I., and Rivers, M. B., "Test summary of the NASA high-lift common research model half-span at QinetiQ 5-metre pressurized low-speed wind tunnel," *AIAA AVIATION 2020 FORUM*, 2020, p. 2770.

[26] Lacy, D. S., and Sclafani, A. J., "Development of the high lift common research model (hl-crm): A representative high lift configuration for transonic transports," *54th AIAA Aerospace Sciences Meeting*, 2016, p. 0308.

[27] Goc, K., Bose, S. T., and Moin, P., "Large Eddy Simulation of the NASA High-Lift Common Research Model," *AIAA SCITECH 2022 Forum*, 2022, p. 1556.

[28] Poinsot, T., and Lelef, S., "Boundary conditions for direct simulations of compressible viscous flows," *J. Comput. Phys.*, Vol. 101, No. 1, 1992, pp. 104 – 129. https://doi.org/https://doi.org/10.1016/0021-9991(92)90046-2.